Please cite this article in press as: Cui et al., Length of mucin-like domains enhances cell-Ebola virus adhesion by increasing binding probability, Biophysical Journal (2021), https://doi.org/10.1016/j.bpj.2021.01.025

Biophysical *Journal*
Article

Biophysical Society

Length of mucin-like domains enhances cell-Ebola virus adhesion by increasing binding probability

Xinyu Cui,[1] Nicole Lapinski,[2] Xiaohui (Frank) Zhang,[1,3] and Anand Jagota[1,2,*]
[1]Department of Bioengineering; [2]Department of Chemical and Biomolecular Engineering; and [3]Department of Mechanical Engineering and Mechanics, Lehigh University, Bethlehem, Pennsylvania

ABSTRACT The Ebola virus (EBOV) hijacks normal physiological processes by apoptotic mimicry to be taken up by the cell it infects. The initial adhesion of the virus to the cell is based on the interaction between T cell immunoglobulin and mucin domain protein, TIM, on the cell surface and phosphatidylserine (PS) on the viral outer surface. Therefore, it is important to understand the interaction between EBOV and PS and TIM, with selective blocking of the interaction as a potential therapy. Recent experimental studies have shown that for TIM-dependent EBOV entry, a mucin-like domain with a length of at least 120 amino acids is required, possibly because of the increase of area of the PS-coated surface sampled. We examine this hypothesis by modeling the process of TIM-PS adhesion using a coarse-grained molecular model. We find that the strength of individual bound PS-TIM pairs is essentially independent of TIM length. TIMs with longer mucin-like domains collectively have higher average binding strengths because of an increase in the probability of binding between EBOV and TIM proteins. Similarly, we find that for larger persistence length (less flexible), the average binding force decreases, again because of a reduction in the probability of binding.

SIGNIFICANCE This work studies the mechanism of TIM-dependent adhesion of the Ebola virus to a cell. Through coarse-grained modeling, we show that longer TIM stalks adhere more easily because they can sample a larger area, thus offering a mechanistic interpretation of an experimental finding. Better mechanistic understanding can lead to therapeutic ideas for blocking adhesion.

INTRODUCTION

A critical step in the life cycle of a viral particle is its adhesion to and uptake by the cell it infects (1,2). A virus usually accomplishes this by hijacking normal physiological processes such as endocytosis, phagocytosis, and macropinocytosis (3–6). Ebola virus (EBOV), one of the filoviruses, is a single strand, negative-sense RNA virus that can infect a wide range of mammalian cells. Ebola virus disease is a severe and often fatal illness that can cause hemorrhagic fever in humans. This disease was first identified in 1976, with a fatality rate of 50–70%, and has caused over 15,000 deaths (7–10). Recent studies show that a set of cellular proteins and molecular mechanisms are required for the virus to enter host cells (6). The internalization of EBOV is initiated by the interaction between viral surface phosphatidylserine (PS) and host cell receptors (11,12). One type of these receptors is the T cell immunoglobulin mucin domain (TIM) family proteins, TIM-1 and TIM-4 (but not TIM-3). Specifically, attachment involves interaction between TIM proteins and phosphatidylserine molecules displayed on the viral surface (Fig. 1 *a*; (1,2,13–15)). Once this binding occurs, the virus is internalized into endosomes mainly via macropinocytosis. Therefore, blocking the binding of EBOV to its host cell could be a promising therapy (16). However, a principal difficulty for designing therapies against viruses lies in the fact that any attempt to block the binding of a virus to a cell surface is likely also to deleteriously affect normal physiological processes, such as the TIM-dependent engulfment of dead cell debris by phagocytes. A better understanding of how physical parameters such as stiffness, length, and ligand density influence the receptor-mediated virus uptake could potentially aid in the development of better antiviral strategies (11,16).

Human TIM proteins (Fig. 1 *b*) are a family of type 1 transmembrane receptors widely expressed on cells in the immune system, including T and B lymphocytes, dendritic cells, and macrophages (17). The IgV and mucin-like domain (MLD, the stalk presenting the ligand-binding IgV domain) comprise the TIM ectodomain and serve essential

Submitted July 2, 2020, and accepted for publication January 20, 2021.
*Correspondence: anj6@lehigh.edu
Editor: Alan Grossfield.
https://doi.org/10.1016/j.bpj.2021.01.025

Please cite this article in press as: Cui et al., Length of mucin-like domains enhances cell-Ebola virus adhesion by increasing binding probability, Biophysical Journal (2021), https://doi.org/10.1016/j.bpj.2021.01.025

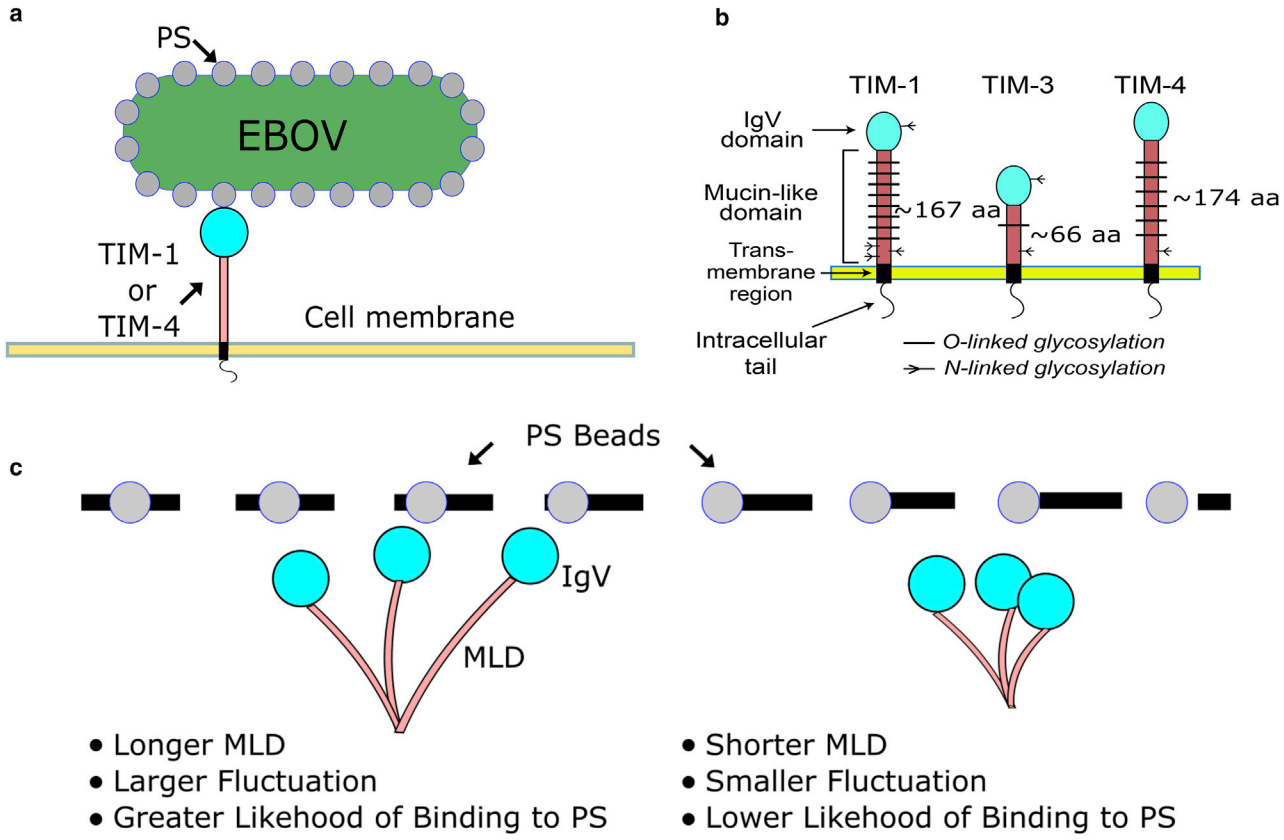

FIGURE 1 (*a*) Simplified model for initiation of EBOV uptake (4,5,9). (Drawings are schematic and not to scale.) EBOV encounters potential host cells and attaches to TIM-1 or TIM-4 on the cell surface via phosphatidylserine. (*b*) Human TIM protein family is shown. The extracellular portion of human TIM is highly conserved, with an N-terminal IgV domain adjacent to a mucin-like domain (MLD). The IgV domain contains a PS-binding metal-ion-dependent ligand-binding site. The MLDs of TIM-1 and -4 are highly glycosylated (57 and 41 predicted O-glycosylation sites, respectively), resulting in a bulky, unstructured, and negatively charged macroglycopeptide region. TIM-2 (data not shown) is found only in mice. (*c*) A hypothesis to explain the advantage of longer MLDs for adhesion is given: the longer the MLD, the larger the region explored by the IgV domain because of thermal fluctuations, and in turn, the larger the region explored, the greater the likelihood of IgV binding to PS. To see this figure in color, go online.

functions in EBOV uptake. The role of the MLD is poorly understood. The size of the MLD varies among the different TIM family members, with TIM-3 having a short MLD (66 amino acids (AAs)) compared with the longer TIM-1 (167 AAs) and TIM-4 (174 AAs). Recent studies show that MLD length plays a role in TIM-PS binding and that MLDs of at least 120 AAs are required for sufficient EBOV uptake (16).

One hypothesis to explain the observed effect of MLD length on TIM-PS adhesion is that with increased length comes increased flexibility in the MLD stalk, effectively increasing the region of the viral surface that can be explored by IgV and possibly increasing the likelihood of forming adhesive bonds (Fig. 1 *c*; (12)). In this work, we examine this hypothesis by developing a coarse-grained computational model of a single TIM stalk interacting with a plane of PS beads. We simulate the process of binding and separation of the two as a function of three parameters: MLD length, MLD flexibility, and PS density. In all cases, we find that the adhesion strength of a single IgV-PS interaction, as measured by the force required to separate IgV from PS, is essentially unchanged if preceded by a binding event. The probability of binding itself depends strongly on each of the three parameters, with the net effect that an increase in average separation force with increasing MLD length is essentially entirely due to a larger probability of binding to a PS bead.

METHODS

We simulated the process of adhesion and separation by first constructing a coarse-grained model of the TIM-PS system (Fig. 2). Our model captures the essential physical features required to examine the hypotheses that the observed effect of MLD length on TIM-PS adhesion is due to the fact that with increased length comes increased flexibility in the MLD stalk. The model includes 1) a plane embedded with PS molecules located a specified distance apart, represented by a single bead each; 2) the terminal IgV domain of the TIM protein, represented by a large bead; and 3) the stalk-like MLD represented by a string of connected beads. The model further includes a bead to represent an atomic force microscopy (AFM) tip.

Multiple potentials were applied to the system, as described below and summarized in Table 1 (see Supporting materials and methods for further details). The adhesive interaction between IgV and PS was represented by a Born-Mayer-Huggins function with a potential depth of 50 k_BT (300 K)

Please cite this article in press as: Cui et al., Length of mucin-like domains enhances cell-Ebola virus adhesion by increasing binding probability, Biophysical Journal (2021), https://doi.org/10.1016/j.bpj.2021.01.025

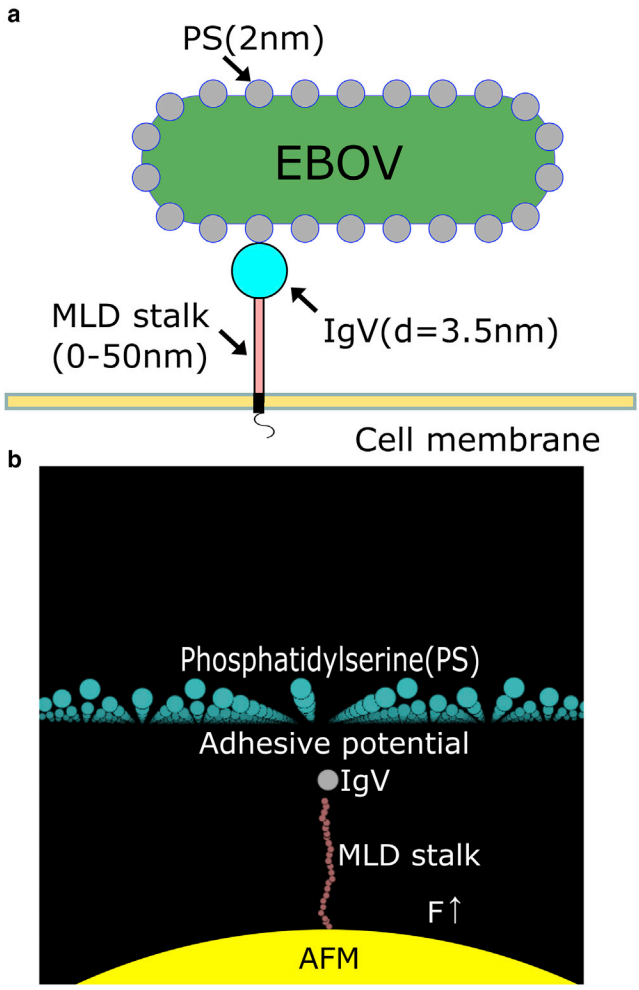

FIGURE 2 A coarse-grained model that captures the main physical features of TIM-PS interaction. (*a*) The essential features are shown schematically (not to scale). They comprise a host membrane in which the TIM receptor is embedded, which binds to phosphatidylserine on the virus surface via the IgV bead. (*b*) Coarse-grained representation comprising 1) a single IgV bead, 2) a string of MLD beads, 3) a single bead representing an AFM force probe subjected to force *F*, and 4) an array of PS beads embedded in a plane representing the viral surface is given. To see this figure in color, go online.

and a minimum of potential at 3.5 nm (to match equilibrium distance of separation without external load (18) and experimental values of pull-off force; see Supporting materials and methods). The PS spacing was chosen to lie between 5 and 20 nm to represent its physiological density in the cell membrane (details in Supporting materials and methods). The MLD was taken to be an inextensible worm-like chain (19,20) and was therefore represented by a string of connected beads ($D_{MLD} = 1$ nm) (21) with stiff spring potentials between adjacent beads and bending potential for each set of three adjacent beads. The spring constant K_s was set at a high value (100 N/m) to constrain the interbead distances to be near their natural length L_0 (22). The bending constant k_θ was in a range set by the MLD stalk's known persistence length (21) and the minimum of the bending potential was at an angle θ_0 of 180°, i.e., for a collinear configuration of the three beads. This is consistent with the fact that there is no evidence that the MLD stalk has any natural curvature, and hence, beads should be collinear at minimal energy. Because we simulate the system using Brownian dynamics, the choice of bead mass is irrelevant (23); it needed to be specified only because it is a required input parameter for LAMMPS (large-scale atomic/molecular massively parallel simulator). A background long-range repulsion from the PS plane against all the beads was used to represent repulsion from glycoproteins on the viral surface between PS beads that prevented any of the MLD beads from penetrating the virus membrane. One additional bead with a large diameter ($D = 50$ nm $>> D_{IgV} = 3.5$ nm, where the diameter of IgV was estimated from its crystal structure (18)) was placed above the PS plane to ensure that the IgV bead did not cross the membrane. We additionally included repulsion between MLD-MLD and MLD-IgV beads to establish self-avoidance. A single simulation began with the TIM beads being pushed toward the PS plane and ended with them being pulled away. This was achieved by attaching the lowest MLD bead to a large bead (e.g., representing an AFM tip ($D_{AFM} = 40$ nm, comparable with an AFM tip) (24)), mimicking a single-molecule AFM experiment (25–28). A time-dependent force was applied to this AFM bead to drive the process of approach and retraction of TIM from the PS plane. All beads had a mass associated with them, as required by the LAMMPS molecular modeling program. However, because we conducted Brownian dynamics simulations, in which bead inertia is neglected, our results did not depend on the choice of these values. This is explained further in the Supporting materials and methods.

Using the model just described, we simulated the time-dependent process in which the TIM receptor is driven by the AFM bead toward the PS surface and then retracted (as might occur in a single-molecule AFM experiment) (25). The adhesive potential depth was adjusted to 50 k_BT to bring the computed pull-off forces within an experimentally relevant range at the loading rate used in the simulation. The model was implemented and simulated through LAMMPS (29,30), and the results were analyzed using scripts written in MATLAB (The MathWorks, Natick, MA) and Visual Molecular Dynamics (31).

A time-dependent force over a range of loading rates was applied to establish a range of pull-off forces. Then, for the majority of simulations in which parameters were varied, we used a loading rate of 0.5 mN/s for 170 ns and then −0.5 mN/S for 830 ns. The former positive loading rate represents pushing the TIM molecule toward the PS plane, and the latter represents pulling the molecule away.

Fig. 3 shows six snapshots from a typical simulation. Fig. 3 *a* (t = 0 ns) represents the initial state in which the MLD beads are arranged in a straight line and the ramp force has just begun to be applied to the large yellow (AFM) bead. At t = 100 ns, the force applied to the AFM bead has pushed up the lower end of the MLD chain. At t = 150 ns, the MLD chain has been pushed against the PS-embedded surface. In this case (but not in all), the IgV bead binds to one of the PS beads on the viral surface. At t = 450 ns, the AFM bead is now subjected to a pulling force. The MLD has started to be pulled with the IgV bead still bound to the PS bead. At t = 600 ns, with continually increasing pulling force, the MLD length starts to be stretched but the IgV bead is still bound to a PS bead. At t = 800 ns, the unbinding process has completed, and the IgV-MLD chain is pulled away from the PS plane. We provide two videos, one representing the cases in which the IgV bead does and a second one for cases in which it does not bind to a PS bead during this process (Videos S1 and S2).

Before conducting production simulations, we needed 1) to establish a loading rate that resulted in appropriate values for the pull-off force, 2) to confirm that the pulling rate was sufficiently slow so the pull-off force was governed by the kinetics of hopping over the energetic barrier and not by the drag force, and 3) to establish a criterion by which we determined whether the IgV bead did or did not bind to a PS bead before being pulled away. In Fig. 4, we plot the distance of several beads from the PS plane as a function of pulling time. The number in the legend represents the bead number such that "1" corresponds to the IgV bead and "50" is the bottom MLD bead attached to the AFM bead. We found that at this chosen rate, the distance versus time plot for bead 1 remained relatively unchanged until ~500 ns of pulling, which corresponded to the IgV bead being bound to a PS bead for some time before dissociating from it. In contrast, the bottom MLD bead was pulled down immediately when the pulling force is applied, but it also had an intermediate plateau, during which period the molecule

Please cite this article in press as: Cui et al., Length of mucin-like domains enhances cell-Ebola virus adhesion by increasing binding probability, Biophysical Journal (2021), https://doi.org/10.1016/j.bpj.2021.01.025

TABLE 1 Parameters for potentials and forces in the coarse-grained model

Beads				
Bead type		**Diameter (nm)**		
PS		2		
MLD		1		
IgV		3.5		
Large bead		50		
AFM bead		40		
Harmonic bond		$E_{spring} = k_s(r - r_0)^2$		
Between		k_s **(N/m)**		r_0 **(nm)**
MLD-MLD		100		1
IgV-MLD		100		3.5
MLD-AFM		100		40
Harmonic angle		$E_\theta = k_\theta(\theta - \theta_0)^2$		
Between		k_θ **(J/°^{2})**		θ_0 **(°)**
IgV-MLD-MLD		5.1455e−21		180
MLD-MLD-MLD		2.0582e−22		180
PS density				
Distance between adjacent PS		5–20 nm		
IgV-PS adhesive potential		$E = Aexp\left(\frac{\sigma - r}{\rho}\right) - \frac{C}{r^6} + \frac{D}{r^8}$		
A (J)	σ **(m)**	ρ **(m)**	**C (J × m^6)**	**D (J × m^8)**
4.116e−20	3.600e−9	2.200e−10	4.693e−70	0
Background long-range repulsion			$F = -F_0 \exp\left(-\frac{Z}{Z_0}\right)$	
F_0 **(nN)**			Z_0 **(nm)**	
1			1	
Large bead repulsion			$E = Aexp\left(\frac{\sigma - r}{\rho}\right) - \frac{C}{r^6} + \frac{D}{r^8}$	
Between	**A (m)**	σ **(m)**	ρ **(m)**	**C (J × m^6)**	**D (J × m^8)**
IgV-large bead	4.116e−20	53.500e−8	2.200e−10	0	0
IgV-AFM	4.116e−20	43.500e−10	2.200e−10	0	0
IgV-MLD	4.116e−20	4.100e−9	2.200e−10	0	0
MLD-MLD	4.116e−20	1.000e−9	2.200e−10	0	0
AFM-MLD	4.116e−20	40.500e−8	2.200e−10	0	0

See text and Supporting materials and methods for justification and explanation.

was stretched but remained bound. This showed that the pulling rate was slow enough for the MLD chain to have sufficient time to sample configurations in the bound state before being pulled off.

Next, we needed to develop a method to calculate the pull-off force and to set up a criterion to distinguish between cases in which unbinding was preceded by an IgV-PS binding event from those in which it was not. The pull-off force was taken to correspond to the time point at which the position of the IgV bead relative to the PS plane became sufficiently large. Specifically, we defined separation as when the IgV-PS-plane distance exceeded twice the equilibrium value of 3.5 nm. Choosing this number between 6 and 10 nm resulted in no qualitative differences and only small quantitative differences in our results. If t^* was the time at which this occurred, the corresponding pull-off force was calculated as

$$f^* = r_f \times t^*, \tag{1}$$

where f^* is the pull-off force, r_f is the constant loading rate, and t^* is the time from the beginning of pulling to the time when unbinding occurred.

Whether the IgV bead was able to find a PS binding partner before being pulled away was easily observed by viewing a video of the simulation. (See Videos S1 and S2.) To determine from the pull-off force whether it corresponded to the removal of a PS-bound or PS-unbound IgV bead, we show in Fig. 5 the distribution of the pull-off force.

It is evident that the distribution is strongly bimodal. The pull-off forces in all the cases in which IgV was not bound to a PS bead before unbinding were below 30 pN. In all the cases in which the two were bound before unbinding, the pull-off forces were greater than 120 pN. Therefore, we could safely identify all the latter cases as those with pull-off force >80 pN and the former cases as those with pull-off force <80 pN.

Finally, we conducted a series of simulations at different pulling rates using a single IgV bead to investigate the rate dependence of pull-off force and to choose a loading rate for the rest of our study. We used the 120 AA MLD as a test example. These simulations began with the IgV-MLD situated under a PS bead at a distance of 3.5 nm. The pushing phase was kept at the loading rate of 0.5 mN/S for 200 ns, but we varied the pulling rate from −0.5 to −10.0 mN/s, repeating each case five times. The average pull-off force is plotted against the logarithm of the pulling rate in Fig. 6.

These results are consistent with the Bell-Evans model with constant loading rate, which predicts that (25)

$$f^* = \frac{k_B T}{\gamma} \ln\left(\frac{\gamma}{k^0 k_B T}\right) + \frac{k_B T}{\gamma} \ln\left(r_f\right), \tag{2}$$

Please cite this article in press as: Cui et al., Length of mucin-like domains enhances cell-Ebola virus adhesion by increasing binding probability, Biophysical Journal (2021), https://doi.org/10.1016/j.bpj.2021.01.025

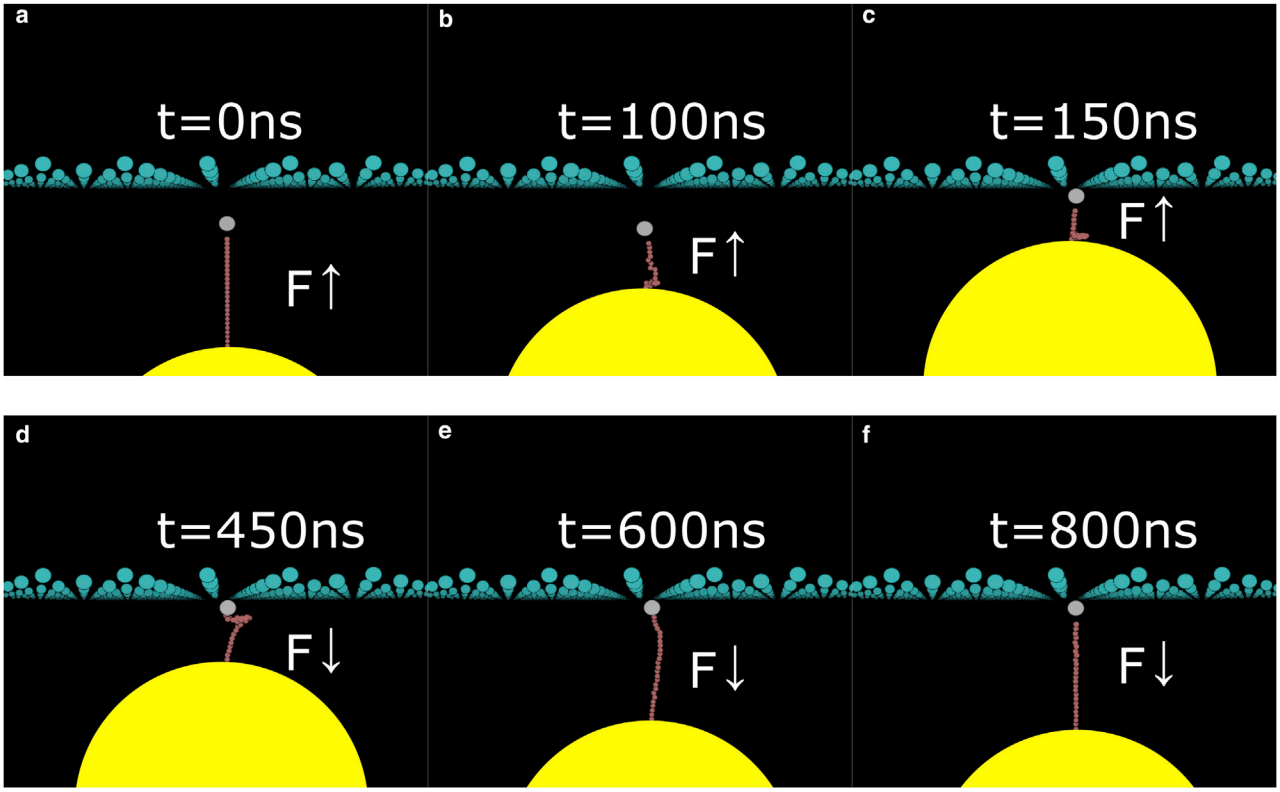

FIGURE 3 Snapshots from different stages of a typical simulation. (*a*) The initial state in which the MLD beads are arranged in a straight line and the ramp force has just begun to be applied is shown. (*b*) The force applied to the AFM bead has pushed the end of the MLD chain, and conformations of the MLD begin to randomize. (*c*) The MLD chain is pushed against the PS-embedded surface. (*d*) The MLD has started to be pulled with the IgV bead still bound to a PS bead. (*e*) The MLD chain begins to be stretched while the IgV bead is still bound to a PS bead. (*f*) The unbinding process is completed, and the IgV-MLD chain is pulled away from the PS plane. Arrows indicate the direction of force applied to the AFM bead. To see this figure in color, go online.

where k_B is Boltzmann's constant, T is the absolute temperature, k^0 is the dissociation rate constant without a pulling force, and γ is the position of the transition state. As predicted by this model, the unbinding force f^* is linear in the logarithm of the loading rate. Moreover, at the lowest loading rate, the pull-off forces were within the range obtained by single-molecule experiments.

The important parameters relevant to the hypothesis we explored in this work that can be varied in our coarse-grained model are the MLD length, MLD persistence length, and PS density. We first explored the effect of the MLD length on the pull-off force, holding the PS density and persistence length constant, by varying the MLD length from 5 to a maximum of 250 AAs. In addition to varying the MLD properties, we also randomly sampled the X-Y location of the lowest MLD bead. We conducted 50 simulations for each MLD length. To study the effect of MLD persistence length, we fixed the PS density and MLD length (120 AAs) but varied the MLD persistence length from 0.01 to 100 nm. Similarly, the effect of PS density was explored by varying the distance between adjacent PS beads with 40 simulations for each PS density. Each case was repeated 35 times.

RESULTS AND DISCUSSION

Effect of MLD length

Fig. 7 shows the results of simulations in which the MLD length was varied. We calculated the average pull-off force in two ways: 1) average over all the simulations, including IgV-PS bound and unbound cases, and 2) average over only those cases in which pull-off was preceded by successful binding of IgV to PS. We also present the probability of IgV-PS binding for each MLD length.

The binding probability increased systematically and significantly with increasing MLD length. This agrees with and supports the hypothesis that a longer MLD length allows sampling of a larger area on the viral surface, resulting in a greater probability of binding. The effect of this on the average pull-off force was striking. The pull-off force, averaged over all simulations, followed the trend set by the probability of IgV-PS binding. In contrast, the pull-off force averaged over only those cases in which IgV-PS binding preceded pull-off showed that the strength of binding, once IgV did bind to PS, was essentially independent of MLD length. Similarly, the average pull-off force for cases in which the IgV did not bind to PS was also constant at a lower value. This is far from obvious because with increasing length, the MLD stalk does sample and attach to PS beads over an increasing area. However, during pulling, the surface adsorbed portion of the MLD chain slides so that just before attachment, the IgV bead is generally directly above the pulling bead. Thus, the process begins with stochastic uncertainty about whether IgV binds to PS. If it does not bind, IgV is pulled off at a very low force.

Please cite this article in press as: Cui et al., Length of mucin-like domains enhances cell-Ebola virus adhesion by increasing binding probability, Biophysical Journal (2021), https://doi.org/10.1016/j.bpj.2021.01.025

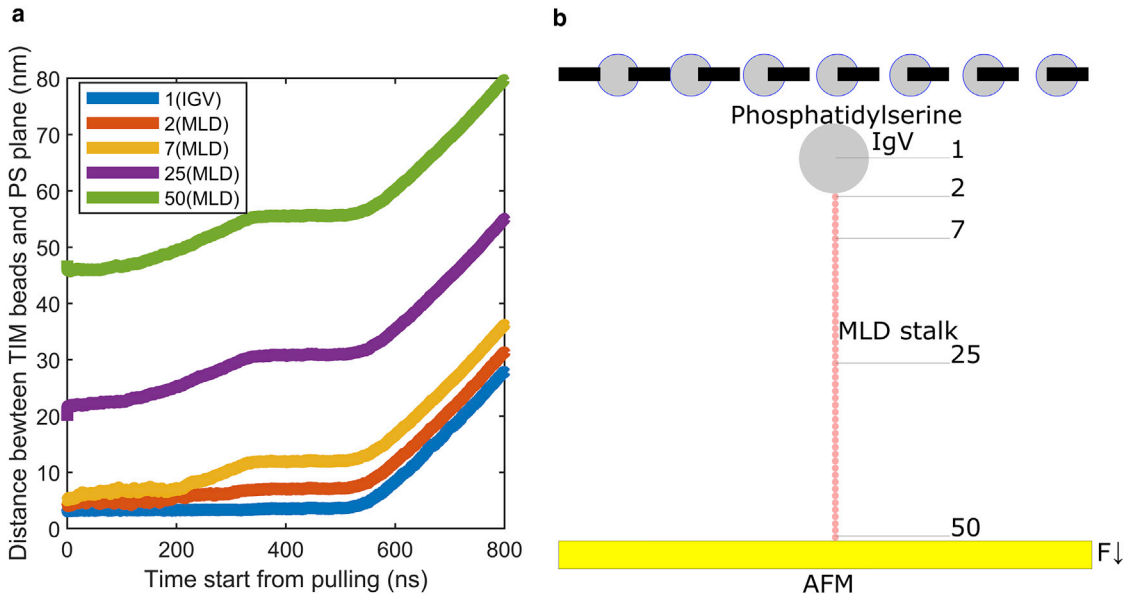

FIGURE 4 (*a*) Demonstration that unbinding is governed by hopping over the energetic barrier rather than drag force: The bottom MLD bead (#50) starts to move once pulling force is applied, whereas the top MLD bead (#2) and IgV (#1) move little until the pulling force reaches a sufficiently large value, which indicates that IgV is captured by the energetic barrier. (*b*) Schematic of unbinding system corresponded to data in (*a*) is given (not to scale). To see this figure in color, go online.

If it does bind, it takes a much larger pull-off force, and in the process, IgV loses its memory of where it first attached. Thus, we can say succinctly that average $F_{pull\text{-}off} = F_{pull\text{-}off}{}^{*} \times Prob(IgV - PS\ binding)$. The first term on the right-hand side, $F_{pull\text{-}off}{}^{*}$, is a property of the binding pair, unaffected by MLD length.

Effect of MLD persistence length

Fig. 8 shows the results for the effect of MLD persistence length on the binding probability and pull-off force. We found that the binding probability decreased systematically with longer MLD persistence length. Evidently, similar to the effect of MLD length, a shorter persistence length means that the more flexible MLD stalk allows IgV to sample a larger area. Precisely as in the case of MLD length, the average pull-off force for cases in which IgV-PS binding precedes unbinding was essentially independent of persistence length. Again, this suggests that the flexible MLD chain fosters binding by facilitating IgV access to a larger region.

Effect of PS density

Fig. 9 shows the effect of PS density on binding probability and pull-off forces. We found that the binding probability decreased with decreasing PS density because of a larger area that the IgV needed to sample to find a PS binding partner. Consistent with the effects of MLD and persistence lengths, the pull-off force averaged over cases in which unbinding was preceded by IgV-PS binding was independent of PS density. Thus, the effect of the decrease in PS density operates by increasing the area that IgV needs to sample.

CONCLUSIONS

In this study, we built a coarse-grained model for the TIM-PS interaction that enable initial EBOV adhesion to cell surfaces. We used the model to examine a hypothesis that explains the experimental finding that MLD stalks longer than a certain length are required for successful TIM-PS binding. The hypothesis we examined posits that longer MLD stalks bind more effectively because they can sample a larger area on the viral surface. That is, even when the binding between a TIM-PS pair is specific, its strength increases with the area that is accessible because of MLD fluctuations when combined with the probability of binding, which increases with area. To examine this hypothesis, we constructed a model in which the MLD was represented by a connected string of beads, terminated at one end by a larger bead representing IgV. We conducted coarse-grained Brownian dynamics simulations of pushing a single TIM receptor against a plane embedded with PS beads, followed by retraction to pull off the TIM away from the PS-embedded surface. We studied the effect of MLD length, persistence length of the MLD, and PS density. It should be noted, however, that TIM-1, TIM-3, and TIM-4 and their allelic variants differ somewhat in structure and PS binding affinity (32). In this work, to focus on the effect of TIM length, we have ignored these differences; i.e., we held the IgV-PS interaction strength at a fixed value. The specific

Please cite this article in press as: Cui et al., Length of mucin-like domains enhances cell-Ebola virus adhesion by increasing binding probability, Biophysical Journal (2021), https://doi.org/10.1016/j.bpj.2021.01.025

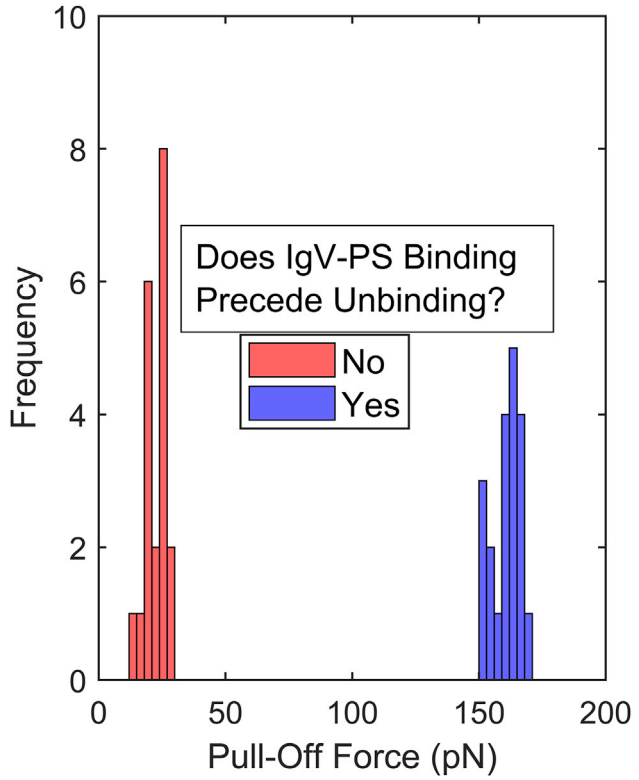

FIGURE 5 Criterion to determine whether unbinding was preceded by an IgV-PS binding event. Pull-off forces clearly fell into two distinct and separate classes. When unbinding was preceded by an IgV-PS binding event, pull-off forces were always >120 pN. Conversely, when unbinding was not preceded by IgV-PS binding, pull-off forces were always <30 pN. Therefore, a threshold value of pull-off force between 30 and 120 pN could safely be used to classify each simulation according to whether or not unbinding was preceded by an IgV-PS binding event. To see this figure in color, go online.

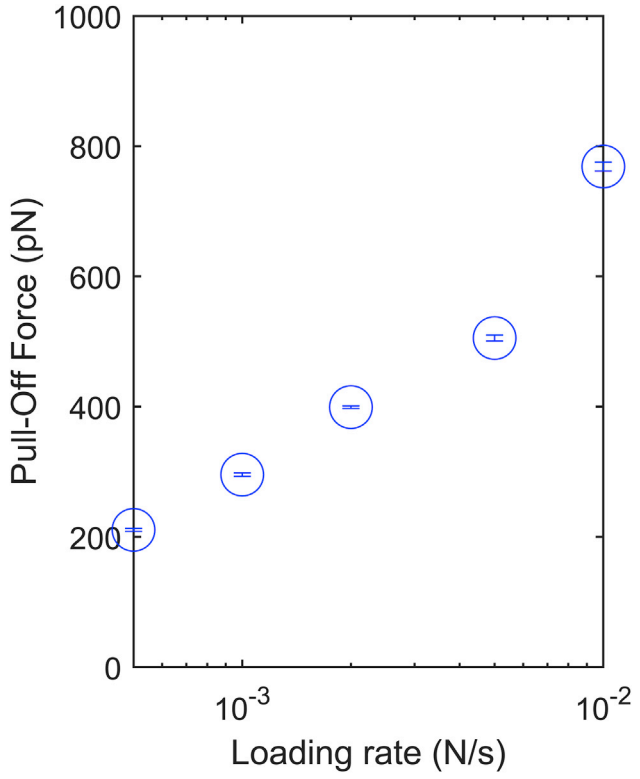

FIGURE 6 Average pull-off forces for different loading rates are plotted against the corresponding loading rates. The plot shows that the pull-off force is approximately linear in the logarithm of the loading rate. Error bars show standard deviation. To see this figure in color, go online.

dependence of the interaction can be included in more detailed models.

We found that increase in MLD length, decrease in MLD persistence length, and increase in PS density all increase the probability of IgV-PS binding. However, the pull-off force, once IgV-PS are bound to each other, remains unchanged. The results are consistent with the experimental finding that longer MLD is needed for successful TIM-PS binding. It also supports the hypothesis that increasing length of MLD is needed to provide flexibility for the TIM stalk to effectively seek binding partners. Smaller persistence lengths and higher PS density have a similar effect on the binding probability. These last two theoretical predictions remain to be tested experimentally. Selective changes in the MLD structure or glycosylation patterns could be used to vary persistence length. Supported bilayers with controlled PS density could be used to verify the effect of PS density. We studied the effects of MLD length, persistence length, and PS density holding the IgV-PS interaction constant. In fact, IgV of different TIM proteins are similar, but not identical (16), so in the physiological setting, it is possible that this additional factor plays a role in determining the effect of changing TIM length.

Our work has several limitations. Firstly, our choice of $\theta_0 = 180^\circ$ is made in lack of experimental data. Similarly, and again in the absence of experiments to guide us, we set IgV-MLD interaction to be repulsive to model steric hindrance, ignoring possible attraction between the two. But this attraction, even if weaker than IgV-PS interaction, could decrease the probability of IgV binding to PS. We believe that our model could be improved by basing these parameters on more detailed all-atom molecular dynamics simulations.

In addition, we considered an isolated TIM-MLD stalk. In actuality, TIM is embedded in a brush of other sugar-like molecules. These affect the flexibility of the MLD stalk, which, to a certain extent, could be captured by modulating the persistence length of the MLD. However, these molecules likely also provide steric and electrostatic repulsion against the PS-embedded surface. This is not accounted for in our model and will be examined in future work. Our system is closer to single-molecule AFM experiments, which have been shown to be consistent with experiments. Also, we did not include the glycoprotein (GP) on the Ebola viral membrane because firstly, it has

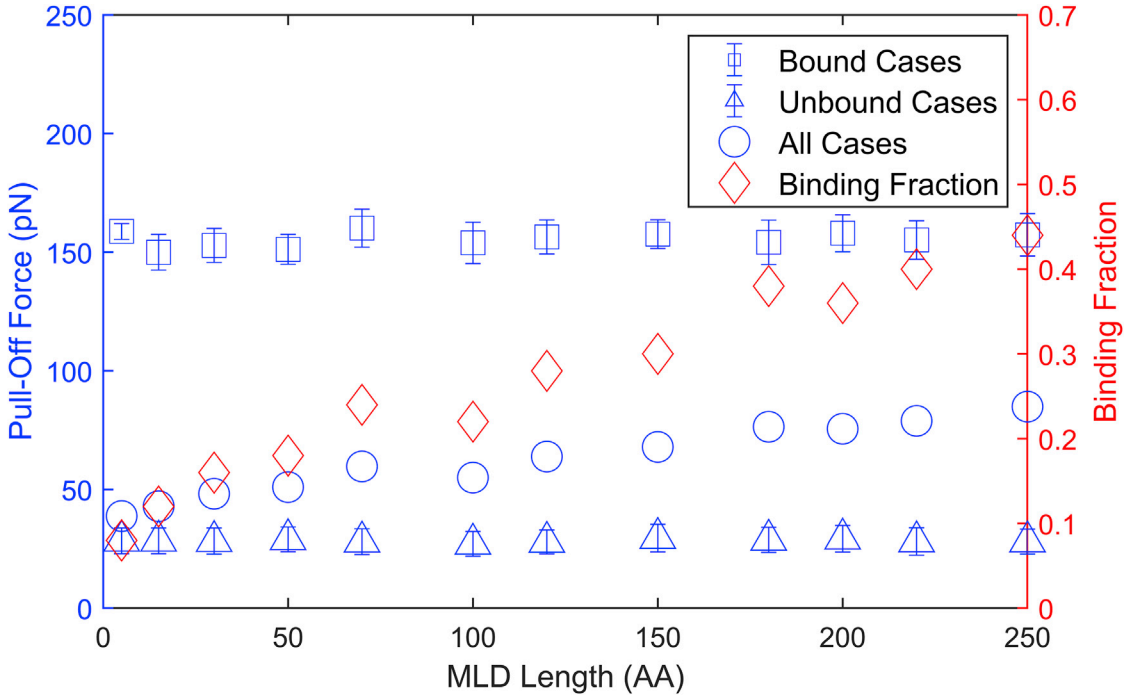

FIGURE 7 The average pull-off force for all cases (*blue circles*) increased with longer MLD. In contrast, the average pull-off force (*blue squares*) for only those cases in which IgV-PS were bound before being pulled apart had roughly a fixed value. Similarly, the average pull-off force (*blue triangles*) for cases in which IgV did not bind to PS had roughly a lower but also fixed value. This indicates that the increase in pull-off force for longer MLDs was essentially entirely due to a higher probability of IgV-PS binding (*red rhombuses*). This supports the hypothesis that increasing MLD length helps to sample and find PS binding partners for IgV. Error bars show standard deviation. To see this figure in color, go online.

been found that the EBOV internalization by TIM-1 is solely PS dependent and does not require the presence of the viral surface glycoprotein (1). Therefore, the main role of the Ebola GP is steric hindrance that is implicitly represented by the energetic barriers created in our model to prevent IgV and MLD beads from crossing the viral membrane surface. Our neglect of the GP is further supported by experimental results that PS-TIM AFM pull-off results on the virus-like particle with and without GP are indistinguishable (25). Possibly, it is difficult for the AFM tip to find a GP because the spacing between Ebola GP is quite large (~200 nm) (33) compared with the AFM tip (20–30 nm). To study the effect of MLD length, we have chosen to fix the IgV domain just as was studied through experiment (12). In applying these results under physiological conditions, one must additionally account for the fact that IgV domains in different TIM proteins are not quite the same (16). Another known receptor for EBOV is Niemann-Pick C1 (NPC1), a late-endosomal membrane protein with little or no expression on the plasma membrane. NPC1 interacts with Ebola GP and mediates the Ebola viral-endosomal membrane fusion. It remains to be clarified whether PS-TIM interaction can function in concert with GP-NPC1 interaction to mediate Ebola endosomal entry (34).

As a coarse-grained model, our work is a drastic simplification because the actual structure of every biological component in our system is far more sophisticated than a collection of beads. Nevertheless, we believe that with judicious choice of coarse-graining model parameters, the essential physical phenomena can be posed and addressed. We believe that our modeling approach contains several elements that can be adapted potentially to study other viruses. By elucidating the mechanisms of adhesion, we hope to spark ideas for therapeutic targets.

SUPPORTING MATERIAL

Supporting Material can be found online at https://doi.org/10.1016/j.bpj.2021.01.025.

AUTHOR CONTRIBUTIONS

X.C. and N.L. developed the model and the codes. X.C. carried out all the simulations and much of the data analysis. A.J. and X.F.Z. designed the study, mentored, and supervised X.C. and N.L., co-interpreted results, and cowrote the manuscript.

ACKNOWLEDGMENTS

We thank the anonymous reviewers for their helpful comments.This work was supported by the National Institutes of Health grant AI133634, by National Science Foundation grant 1804117, and by a Lehigh University internal CORE grant.

Please cite this article in press as: Cui et al., Length of mucin-like domains enhances cell-Ebola virus adhesion by increasing binding probability, Biophysical Journal (2021), https://doi.org/10.1016/j.bpj.2021.01.025

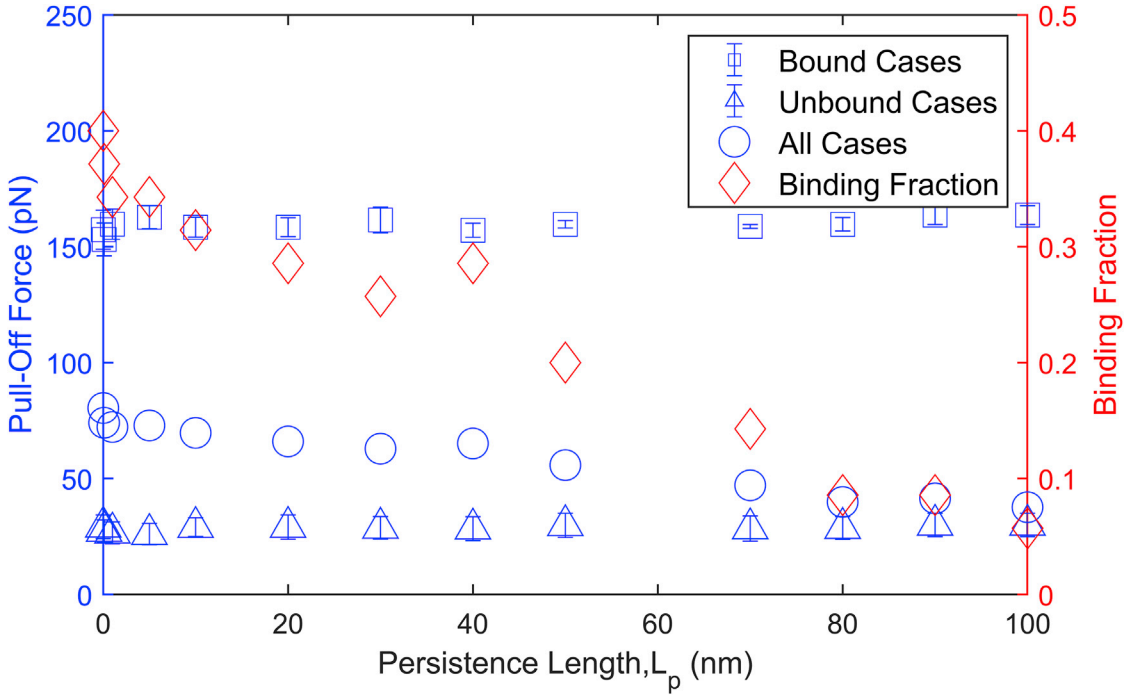

FIGURE 8 The pull-off force averaged over all simulations (*blue circles*) decreased with increasing MLD persistence length. However, the pull-off force averaged over only the simulations in which the IgV bound to PS (*blue squares*) remained roughly unchanged, which indicates that the decrease in the former for a higher persistence length was due to a reduction in the binding probability (*red rhombuses*). That is, a flexible MLD stalk (small persistence length) favors PS-IgV binding. Error bars show standard deviation. To see this figure in color, go online.

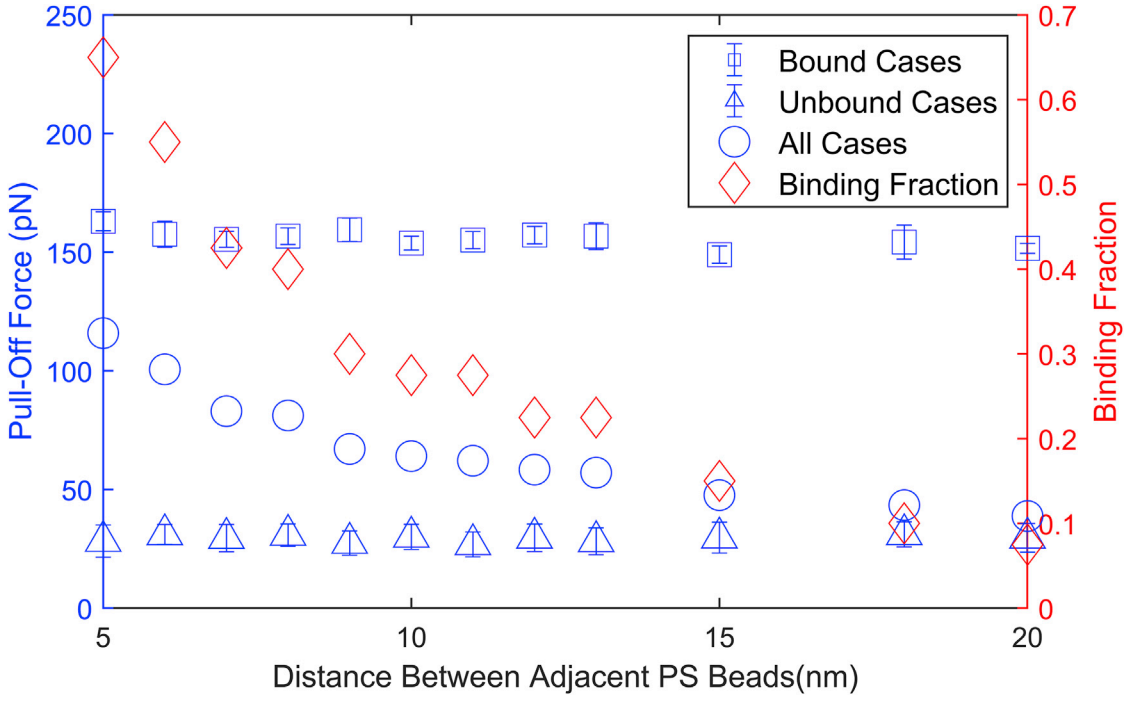

FIGURE 9 Binding probability and average pull-off force for different PS densities. The plot shows that a higher PS density significantly increased the IgV-PS binding probability, whereas the average pull-off force for cases in which IgV-PS binding occurred remained roughly constant. Error bars show standard deviation. To see this figure in color, go online.

Please cite this article in press as: Cui et al., Length of mucin-like domains enhances cell-Ebola virus adhesion by increasing binding probability, Biophysical Journal (2021), https://doi.org/10.1016/j.bpj.2021.01.025

REFERENCES

1. Jemielity, S., J. J. Wang, …, H. Choe. 2013. TIM-family proteins promote infection of multiple enveloped viruses through virion-associated phosphatidylserine. *PLoS Pathog.* 9:e1003232.
2. Moller-Tank, S., and W. Maury. 2014. Phosphatidylserine receptors: enhancers of enveloped virus entry and infection. *Virology.* 468–470:565–580.
3. Nanbo, A., M. Imai, …, Y. Kawaoka. 2010. Ebolavirus is internalized into host cells via macropinocytosis in a viral glycoprotein-dependent manner. *PLoS Pathog.* 6:e1001121.
4. Miller, E. H., and K. Chandran. 2012. Filovirus entry into cells - new insights. *Curr. Opin. Virol.* 2:206–214.
5. Hunt, C. L., N. J. Lennemann, and W. Maury. 2012. Filovirus entry: a novelty in the viral fusion world. *Viruses.* 4:258–275.
6. Takada, A. 2012. Filovirus tropism: cellular molecules for viral entry. *Front. Microbiol.* 3:34.
7. Piot, P., J. J. Muyembe, and W. J. Edmunds. 2014. Ebola in west Africa: from disease outbreak to humanitarian crisis. *Lancet Infect. Dis.* 14:1034–1035.
8. Joob, B., and V. Wiwanitkit. 2014. Ebola outbreak in west Africa. *Afr. Health Sci.* 14:1085.
9. Meyers, L., T. Frawley, …, C. Kang. 2015. Ebola virus outbreak 2014: clinical review for emergency physicians. *Ann. Emerg. Med.* 65:101–108.
10. Gatherer, D. 2014. The 2014 Ebola virus disease outbreak in West Africa. *J. Gen. Virol.* 95:1619–1624.
11. Rhein, B. A., R. B. Brouillette, …, W. Maury. 2016. Characterization of human and murine T-cell immunoglobulin mucin domain 4 (TIM-4) IgV domain residues critical for Ebola virus entry. *J. Virol.* 90:6097–6111.
12. Moller-Tank, S., L. M. Albritton, …, W. Maury. 2014. Characterizing functional domains for TIM-mediated enveloped virus entry. *J. Virol.* 88:6702–6713.
13. Noda, T., H. Ebihara, …, Y. Kawaoka. 2006. Assembly and budding of Ebolavirus. *PLoS Pathog.* 2:e99.
14. Meertens, L., X. Carnec, …, A. Amara. 2012. The TIM and TAM families of phosphatidylserine receptors mediate dengue virus entry. *Cell Host Microbe.* 12:544–557.
15. Rankl, C., F. Kienberger, …, P. Hinterdorfer. 2008. Multiple receptors involved in human rhinovirus attachment to live cells. *Proc. Natl. Acad. Sci. USA.* 105:17778–17783.
16. Moller-Tank, S., A. S. Kondratowicz, …, W. Maury. 2013. Role of the phosphatidylserine receptor TIM-1 in enveloped-virus entry. *J. Virol.* 87:8327–8341.
17. Angiari, S., and G. Constantin. 2014. Regulation of T cell trafficking by the T cell immunoglobulin and mucin domain 1 glycoprotein. *Trends Mol. Med.* 20:675–684.
18. Santiago, C., A. Ballesteros, …, J. M. Casasnovas. 2007. Structures of T cell immunoglobulin mucin protein 4 show a metal-Ion-dependent ligand binding site where phosphatidylserine binds. *Immunity.* 27:941–951.
19. Boal, D. 2012. Mechanics of the Cell. Cambridge University Press, Cambridge, UK.
20. Marantan, A., and L. Mahadevan. 2018. Mechanics and statistics of the worm-like chain. *Am. J. Phys.* 86:86–94.
21. Kramer, J. R., B. Onoa, …, C. R. Bertozzi. 2015. Chemically tunable mucin chimeras assembled on living cells. *Proc. Natl. Acad. Sci. USA.* 112:12574–12579.
22. Round, A. N., M. Berry, …, M. J. Miles. 2002. Heterogeneity and persistence length in human ocular mucins. *Biophys. J.* 83:1661–1670.
23. van Gunsteren, W. F., and H. J. C. Berendsen. 1982. Algorithms for brownian dynamics. *Mol. Phys.* 45:637–647.
24. Maragliano, C., A. Glia, …, M. Chiesa. 2014. Effective AFM cantilever tip size: methods for in-situ determination. *Meas. Sci. Technol.* 26:015002.
25. Dragovich, M. A., N. Fortoul, …, X. F. Zhang. 2019. Biomechanical characterization of TIM protein-mediated Ebola virus-host cell adhesion. *Sci. Rep.* 9:267.
26. Binnig, G., C. F. Quate, and C. Gerber. 1986. Atomic force microscope. *Phys. Rev. Lett.* 56:930–933.
27. Zhang, X., S. E. Craig, …, V. T. Moy. 2004. Molecular basis for the dynamic strength of the integrin alpha4beta1/VCAM-1 interaction. *Biophys. J.* 87:3470–3478.
28. Zhang, X., E. P. Wojcikiewicz, and V. T. Moy. 2006. Dynamic adhesion of T lymphocytes to endothelial cells revealed by atomic force microscopy. *Exp. Biol. Med. (Maywood).* 231:1306–1312.
29. Plimpton, S. 1993. Fast parallel algorithms for short-range molecular dynamics. Sandia National Labs, Albuquerque, NM.
30. Plimpton, S., R. Pollock, and M. Stevens. 1997. Particle-mesh Ewald and rRESPA for parallel molecular dynamics simulations. *In* Proceedings of the Eighth SIAM Conference on Parallel Processing for Scientific Computing, PPSC 1997. Hyatt Regency Minneapolis on Nicollel Mall Hotel, Minneapolis, Minnesota, USA, March 14-17, 1997 (SIAM.
31. Humphrey, W., A. Dalke, and K. Schulten. 1996. VMD: visual molecular dynamics. *J. Mol. Graph.* 14:33–38, 27–38.
32. Freeman, G. J., J. M. Casasnovas, …, R. H. DeKruyff. 2010. TIM genes: a family of cell surface phosphatidylserine receptors that regulate innate and adaptive immunity. *Immunol. Rev.* 235:172–189.
33. Beniac, D. R., and T. F. Booth. 2017. Structure of the Ebola virus glycoprotein spike within the virion envelope at 11 Å resolution. *Sci. Rep.* 7:46374.
34. Kuroda, M., D. Fujikura, …, A. Takada. 2015. Interaction between TIM-1 and NPC1 is important for cellular entry of Ebola virus. *J. Virol.* 89:6481–6493.